ELSEVIER

Journal of Structural Geology 28 (2006) 508–518

JOURNAL OF STRUCTURAL GEOLOGY

www.elsevier.com/locate/jsg

A study of compaction bands originating from cracks, notches, and compacted defects

R. Katsman *, E. Aharonov

Department of Environmental Sciences and Energy Research, Weizmann Institute of Science, Rehovot, 76100, Israel

Received 13 February 2005; received in revised form 4 December 2005; accepted 10 December 2005

Abstract

Compaction bands are zones of localized grain crushing and porosity reduction, which form spontaneously in high porosity rock under certain compressive stress conditions. Recent experiments show that compaction bands may nucleate at the edges of notches, holes and cracks subjected to compressive stress. We present an elasto-plastic model, used to investigate compaction band formation under a variety of boundary conditions. When simulating a notched specimen and a specimen with a central hole, compaction initiated at the macroscopic void's tips, and propagated in a step-wise manner, in agreement with experimental results. This step-wise manner of propagation is different from the compaction band run-away observed when compaction bands nucleate from pre-existing compaction bands. In addition, heterogeneity in rock properties, such as heterogeneity in local compressive strength, was found to control the morphology of compaction features initiating from voids.

Keywords: Rock mechanics; Compaction bands; Porous rock; Spring network model

1. Introduction

Compaction bands (CBs) were recently identified in the field and in laboratory experiments (e.g. Mollema and Antonellini, 1996; Wong et al., 1997, 2001; Rudnicki and Olsson, 1998; Issen and Rudnicki, 2000, 2001), as discrete localized deformation zones, occurring in initially high porosity rocks subjected to high mean and low differential compressive stress. These naturally occurring compaction zones appear perpendicular to the maximum compressive direction, and are formed by grain crushing and porosity reduction.

CBs may play an important role in determining fluid flow, and stress and strain distribution in sedimentary basins. In addition, their importance in controlling borehole stability was recently noted (Haimson, 2001, 2003; Klaetsch and Haimson, 2002; Haimson and Kovachich, 2003). Despite their importance, they are a recently discovered feature and their formation under a variety of boundary conditions is still not well understood.

We recently proposed a new model to investigate CB formation and localization (Katsman et al., 2005). By modeling an elasto-plastic media where localized compression-induced volume reduction is allowed to occur, it was found that locations of compressive stress concentration may act as nucleation sites for compaction bands. The model thus explains how a stiff sample boundary causes CBs to originate at its corners, as in the experiments of Rudnicki and Olsson (1998), Issen and Rudnicki (2000, 2001), Klein et al. (2001), Wong et al. (1997, 2001), and Baud et al. (2004). Then, the CB tip itself operates as a stress concentrator, inducing band growth perpendicular to the maximum compressive stress, and nucleation of other bands downstream, resulting in a CB front propagation.

Moreover, recent field observations and experiments show that CBs may nucleate not only at the edges of the previously-created CBs, but also at the edges of notches, holes, cracks, and other geological structures. Mollema and Antonellini (1996) observed thick CBs specifically in the compressional quadrant near the tip of a shear band. Haimson et al. (citation of 'Haimson et al.' refers to Haimson (2001, 2003), Klaetsch and Haimson (2002), Haimson and Kovachich (2003), and Haimson and Lee (2004)) experimentally observed long and narrow, stress-induced breakouts in the vicinity of boreholes in high-porosity sandstones. Vajdova et al. (2003) and Vajdova and Wong (2003) experimented with aspects of CB nucleation and propagation at the edges of notches cut into a high-porosity sandstone. These field and laboratory observations suggest that in high-porosity rock, the enhanced compressive stress

* Corresponding author. Tel.: +972 8 9344923; fax: +972 8 9344124.
E-mail address: regina.katsman@weizmann.ac.il (R. Katsman).

0191-8141/$ - see front matter © 2006 Elsevier Ltd. All rights reserved.
doi:10.1016/j.jsg.2005.12.007

expected at a breakout or a shear band tip may result in localized grain de-bonding, grain crushing, and formation of a CB. Moreover, both macro- and micro-scale heterogeneities and defects in the real rocks, even sometimes small voids, may initiate CBs, probably due to the stress concentration induced by these defects (Sternlof and Pollard, 2002; Vajdova et al., 2003; Vajdova and Wong, 2003; Tembe et al., in press; Haimson et al.).

To understand the physical mechanism of CB nucleation and propagation in the vicinity of various defects, i.e. preexisting compacted regions and macroscopic voids, the dependence on elastic properties, and the role of disorder in the development of compaction features, we conducted the theoretical investigation presented here. Results indicate that disturbances and defects in elastic matter (preexisting CBs, holes, heterogeneous material properties, and boundary incompatibility) all act as local stress concentrators. In this way, features of one kind, such as open holes, may cause nucleation and propagation of stress-induced features of a completely different nature, in this case CBs. However, since CB propagation depends on the specific features of the stress field, different defects may cause a different propagation pattern.

2. The physical basis for the model

The compaction process usually occurs in rocks with high initial porosity $\phi_{init} > 20\%$ (Olsson, 2001). After compaction, the porosity within the band is measured to be reduced to values of $\phi_{comp} = 10$–20% (Mollema and Antonellini, 1996; Issen and Rudnicki, 2000; Olsson, 2001). The compaction process in high-porosity sedimentary rock can be mechanically described as follows: when a compactive yield stress is exceeded, the sutures and cement between grains break down; the mobility of de-bonded grains in a fabric containing significant porosity allows them to re-pack (Klaetsch and Haimson, 2002), with possible (Mollema and Antonellini, 1996; Vajdova et al., 2003; Vajdova and Wong, 2003; Haimson et al.) intra-granular microcracking (Fig. 1a).

The volume loss associated with observed porosity reduction may be calculated as follows: consider in 3D a unit of rock of length $2c$, height $2H$, and thickness L (perpendicular to the X–Y plane), undergoing compaction, as in Fig. 1a. Before compaction, the unit of porous rock has volume:

$$V_{init} = V_s + V_p = 2c \cdot 2H \cdot L \tag{1}$$

The total initial volume of the unit, V_{init}, is composed of the volume that the solid grains occupy within the rock matrix, $V_s = (1-\phi_{init})V_{init}$, and the volume that the pores occupy $V_p = \phi_{init} \cdot V_{init}$. During compaction, the porosity is reduced from its pre-compacted value, ϕ_{init}, to a post-compacted one, ϕ_{comp}. Since no solid is removed from the unit, V_s remains constant, but the pore volume is reduced to a new value, $V_p^{new} = \phi_{comp} \cdot V_{comp}$. Where V_{comp} is the new total volume of the unit:

$$V_{comp} = \frac{1-\phi_{init}}{1-\phi_{comp}} V_{init} \tag{2}$$

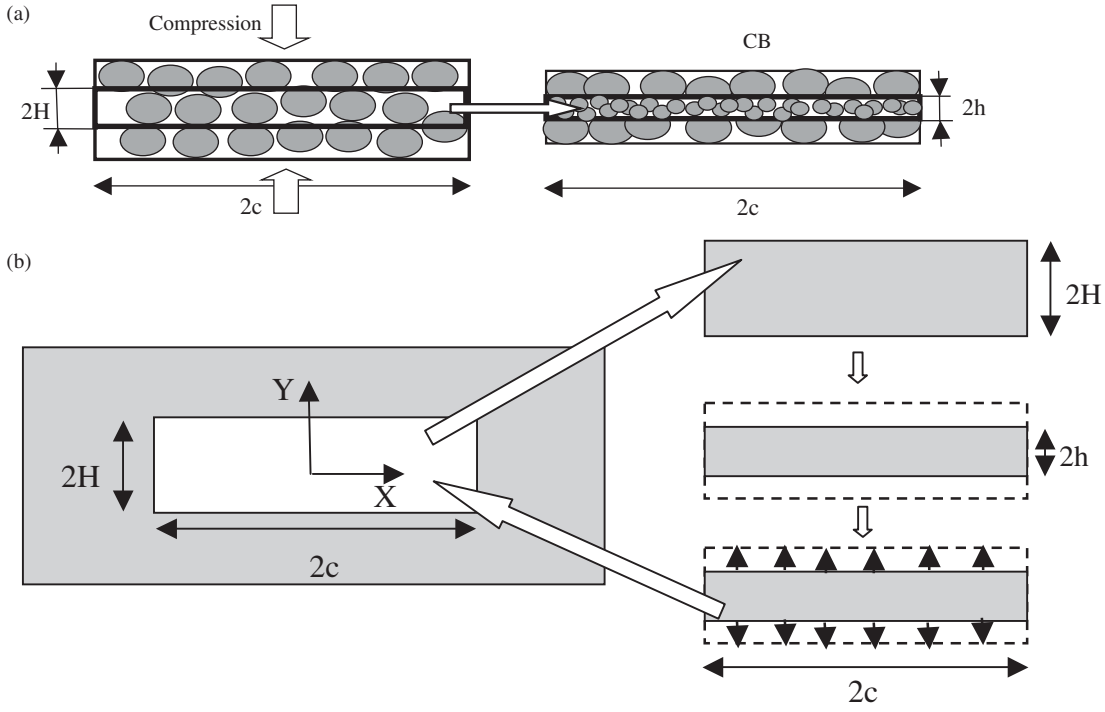

Fig. 1. (a) Compaction band, characterized by vertical dimension shortening ($2H$: before compaction, $2h$: after compaction), and no lateral dimensional changes ($2c$: length of CB before and after compaction process). (b) The transformation problem introduced by Eshelby (1957), applied for the CB studied in the paper. A rectangular region of size $2H \times 2c$ is removed from an elastic body. Then an unconstrained transformation, decreasing the height $2H$ by a value $2(H-h)$ (i.e. volume reduction), took place (CB formation). Its length $2c$ remained unchanged. Vertical surface traction was applied in order to restore the region to its original form. Then the region was glued back into the hole in the matrix. This procedure creates a state of internal stress, which persists even in the absence of external load.

Since compaction is in the vertical (Y) direction, and $L=$ const and $2c=$const before and after compaction, the fraction of the lost volume $1-(V_{comp}/V_{init})$ is equivalent to $(H-h)/H$ (Fig. 1a), where $2h$ is the height of the CB after compaction. As a result, using Eq. (2), the fraction of height removed from the initial height $2H$ is:

$$(H-h)/(H) = \frac{\phi_{init}-\phi_{comp}}{1-\phi_{comp}} \quad (3)$$

Taking characteristic values for porosity within a CB prior and after compaction $\phi_{init}=0.25$ and $\phi_{comp}=0.13$, and plugging into Eq. (3), one obtains $(H-h)/H=0.14$, i.e. 14% of the initial height was lost during a CB creation.

The compaction process is actually a transformation that causes localized irreversible vertical shortening (Fig. 1b). Eshelby, in his classical paper from 1957 (Eshelby, 1957), formulated an analytical method to calculate internal stresses that arise from localized irreversible volume changes within elastic media. Specifically for the CB geometry, a rectangular region of size $2H\times 2c$ is removed from an elastic body (Fig. 1b). Then an unconstrained transformation, decreasing the height $2H$ by a value $2(H-h)$ (CB formation), takes place. Its length $2c$ and thickness L (perpendicular to the X–Y plane) remain unchanged. Surface traction must be applied in order to restore the region to its original dimensions. After this 'stretching', the region is glued back into the hole in the matrix. This procedure of CB origination (which follows Eshelby's formulation) creates a state of internal stress, which persists even in the absence of external load. Under load, the internal stress continues to affect the surrounding stress field. The connection between Eshelby's problem and CBs, stylolites and even deep earthquakes, is further detailed in Katsman et al. (in press).

3. Model

The basic model used is a version of a spring network model (SNM), which was adapted by us to model compaction. SNMs were initially used to investigate crack nucleation, propagation, and growth of crack networks. SNMs are especially suitable for modeling highly heterogeneous matter, defects, and sharp discontinuities in material properties (Curtin and Scher, 1990a,b). A detailed description of the model and the algorithm used is given in Katsman et al. (in press). Briefly, a two-dimensional elastic material is represented as a lattice of nodes connected in a regular hexagonal (triangular) array. A central force spring model is used, where the springs can transfer only normal forces (neither shear force nor moment is incorporated). To avoid lattice artifacts that emerge when using single springs as the basic unit, we use instead the symmetric triangular unit of three springs as the basic unit for the calculations (see Appendix A for details).

The nodes are linked by elastic Hookian springs, characterized by Young's modulus (E), cross-sectional area (A), equilibrium length in a relaxed position (l^{eq}) (these variables are put into dimensionless form and set equal to unity), and prescribed stress thresholds in extension and compression (σ_e, σ_c). Since spring length is dimensionless, it may represent any length. Here each spring is chosen to represent a collection of about 5–10 grains, an average thickness of a CB (Klaetsch and Haimson, 2002; Haimson and Kovachich, 2003).

The force acting on a spring connecting nodes i–j is proportional to the springs expansion or contraction. This force is linearly related to the departure of the length, l, from its equilibrium value, l^{eq}:

$$F_{ij} = F_{ji} = \alpha_{ij}(l-l^{eq})_{ij};\ \alpha_{ij} = \frac{E_{ij}A_{ij}}{l_{ij}^{eq}} \quad (4)$$

Positive (negative) force corresponds to an expanded (contracted) spring. Stress and force on the springs are equivalent here, since A is taken as 1 in Eq. (4).

A new addition to the SNM model (Katsman et al., 2005) allows modeling compaction as a process of local volume reduction: triangular elements that experience a vertical compressive stress larger than a prescribed threshold in compression, σ_c, undergo compaction, modeled by reduction of the equilibrium length of the two non-horizontal springs of the unit. The amount of vertical shortening that the unit experiences, $2(H-h)$, reflects its porosity loss during compaction (Fig. 1; Eq. (3)). Thus, each compacted unit basically undergoes an Eshelby-type volume reducing transformation (Eshelby, 1957), as detailed in Katsman et al. (in press), and in the previous section. Young's modulus of those springs can also be changed if we choose to do so, to simulate compaction hardening or softening. Moreover, after changing the equilibrium length of the non-horizontal springs of the lattice, the elastic modulus of the horizontal spring of the altered unit is iteratively tuned so that its length remains equal to its value before the changes. This procedure ensures that negligible shear motion (in the X direction) accompanies the vertical compaction transformation (see Mollema and Antonellini (1996) and Olsson (2001) for CBs characteristics).

As in other SNM models of cracking (e.g. Curtin and Scher, 1990a,b; Schlangen and Garboczi, 1996, 1997), triangular elements that experience a vertical extensive stress larger than a prescribed threshold in extension, σ_e, break. Breakage is modeled by changing to zero the elastic modulus of the springs. To treat both compaction and breaking processes, a force-couple is applied to the end-points of each altered spring, as explained in Katsman et al. (2005). Verification of the model was conducted as detailed in the Appendix of Katsman et al. (in press).

Disorder and heterogeneity in material properties are introduced by using a random Gaussian probability distribution of stress thresholds among the units:

$$P(\sigma) = \frac{2}{\pi\Delta\sigma}e^{-(\sigma-\bar{\sigma})^2/\Delta\sigma^2} \quad (5)$$

where σ is the stress threshold for each unit, $\Delta\sigma$ is the half-width of the stress threshold distribution, and $\bar{\sigma}$ is the centered value of the distribution.

The degree of disorder in a specific simulation is characterized by:

$$D = |\Delta\sigma/\bar{\sigma}| \quad (6)$$

In the simulations reported here, a lattice of 101×50 was utilized. Samples were initiated with a prescribed defect with a given length of either $2c$ for a central hole or c for notches, and with a height of 1 unit. Notches and holes are defined as regions having non-horizontal springs with a zero Young's modulus, $E_{new} = 0$. The initial compaction defect is prescribed by setting $l^{eq} = 0.9$ and $E_{new} = 1.5$ to non-horizontal springs in a few adjacent units.

In the models presented below, constant strain rate loading is modeled quasi-statically. Simulations start from a completely relaxed equilibrium position of the lattice with prescribed defects when displacements of the external boundaries equal zero and forces in each spring measured by Eq. (4) are zero as well. Then the external boundary conditions are applied to the bottom and top surfaces by prescribing a desired macroscopic strain in the Y-direction. Constant horizontal pressure is applied to the lateral boundary nodes.

As a result of this boundary displacement, both elastic and inelastic (plastic) responses of the matrix might be required to reach a new equilibrium. After all springs with stress values exceeding σ_e and σ_c have been broken and compacted, respectively, a new equilibrium position is reached. At this new equilibrium, it is possible that additional springs experience stress above the thresholds. If so, these springs are compacted/broken as needed, and the procedure is repeated until no more springs exceed the thresholds. Keeping displacements small enough, the new equilibrium position for each internal and boundary node is found at each stage of the calculations.

4. Conditions

The first set of simulations (Fig. 2, top) represents a homogeneous sample with a previously-created CB in its midst. The second set of simulations (Fig. 3, top) represents a homogeneous sample with a thin hollow flaw (crack) in its midst, a setup similar to that used in the experiments of Haimson et al. (a thin hollow flaw might also represent an elliptical borehole with a major axis much longer then the minor one). The third set of simulations (Fig. 3, bottom), represents a homogeneous media with thin notches cut into the lateral boundaries, as in the experiments of Vajdova et al. (2003) and Vajdova and Wong (2003). In all the simulations, compressive vertical strain was applied incrementally to the horizontal boundaries to simulate continuous loading. Constant stress was also applied to the vertical boundaries. No boundary elastic mismatch was incorporated. As vertical compression progressed, some of the units in the lattice underwent compaction. To simulate compaction, the equilibrium length of springs experiencing $\sigma > \sigma_c$ was changed from the initial value of $l^{eq}_{old} = 1$ to a new one of $l^{eq}_{new} = 0.9$, while their Young's modulus was increased from $E_{old} = 1$ to $E_{new} = 1.5$. These values were chosen following reports on 10–20% porosity reduction (Klein et al., 2001; Olsson, 2001), and hardening (i.e. Young's modulus increase; Issen and Rudnicki, 2000), measured in localized compaction.

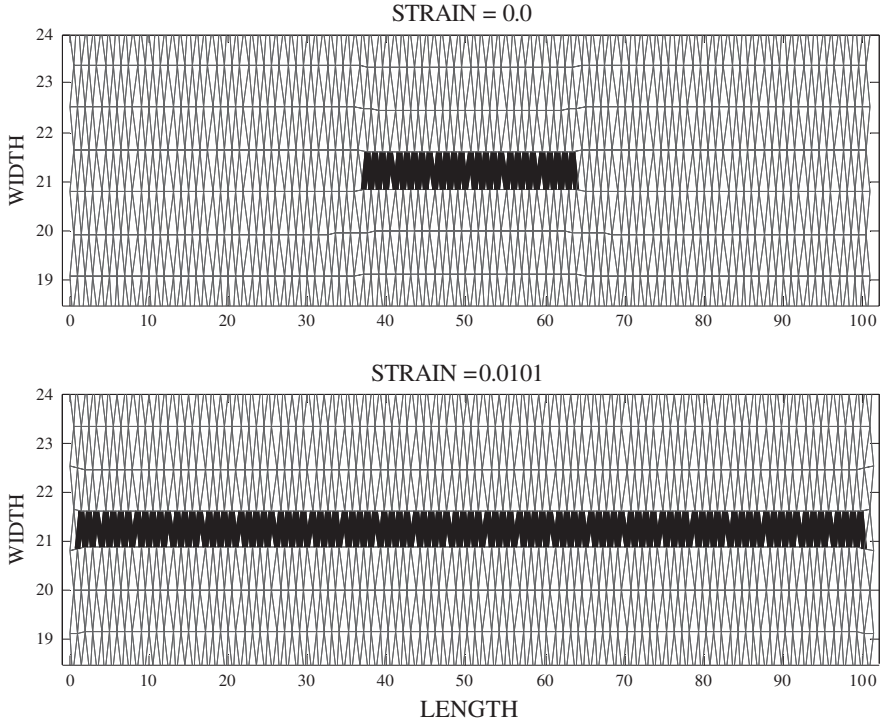

Fig. 2. (top) Initial conditions: planar CB prescribed in the middle of a homogeneous specimen (D = 0); (bottom) CB propagates from the initial CB tip across the entire specimen toward the lateral boundaries in a runaway mode, compacting a whole row.

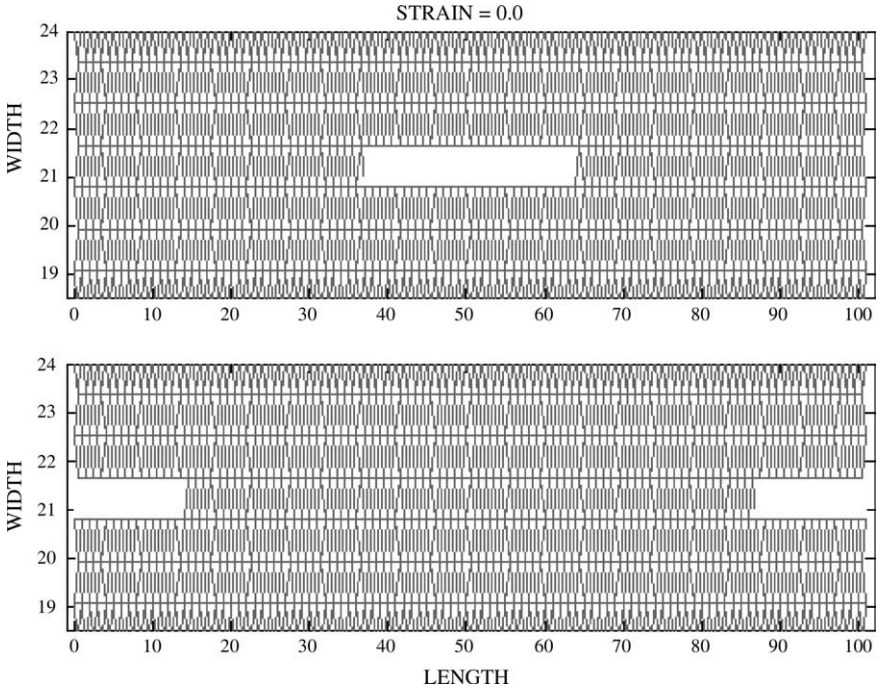

Fig. 3. Initial conditions: (top) a planar hole of length $2c$, cut in the middle of a specimen; (bottom) two notches, each of length c, cut into the lateral boundaries of a specimen. Compressive strain boundary conditions are applied to the horizontal boundaries. Compressive stress boundary conditions are applied to the vertical boundaries.

5. Results

5.1. Compaction bands in a specimen with an initial CB

Fig. 2 presents development of CBs induced by an initial central CB of length $2c$, in a specimen undergoing compression. It was found in the simulations that once the remote strain was increased beyond a critical value (0.0101), a CB propagates from the initial CB tip across the entire specimen towards the lateral boundaries, in a run-away mode (as in Fig. 5, top), compacting a whole row under the same remote strain.

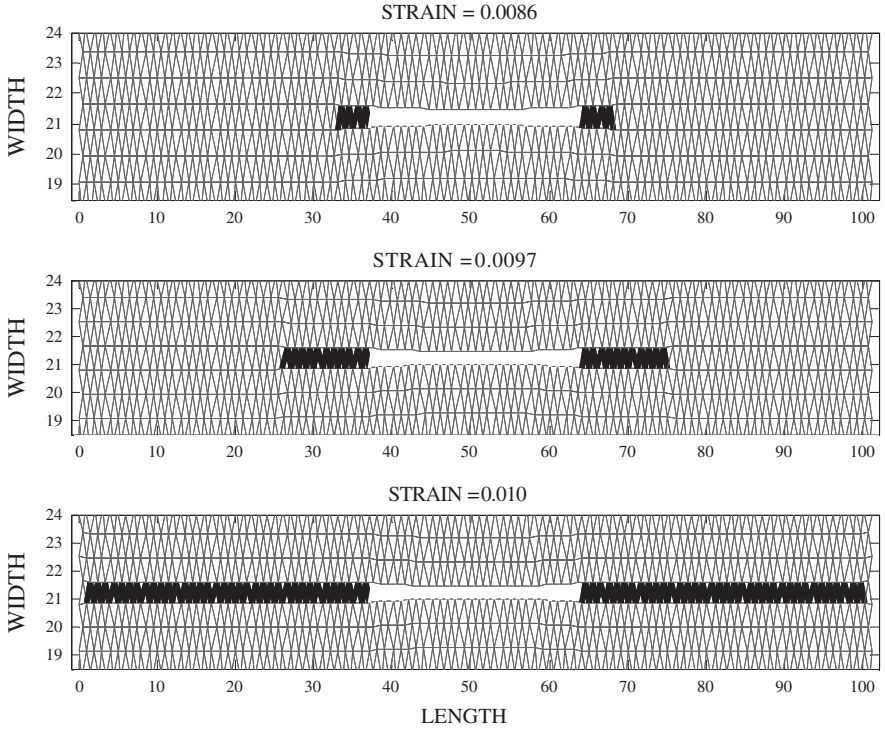

Fig. 4. Progressive development of compaction bands nucleating from a planar flaw cut in the middle of a homogeneous ($D=0$) specimen. Compaction bands develop perpendicular to the maximum compressive direction, and propagate incrementally with increasing strain, towards the lateral boundaries.

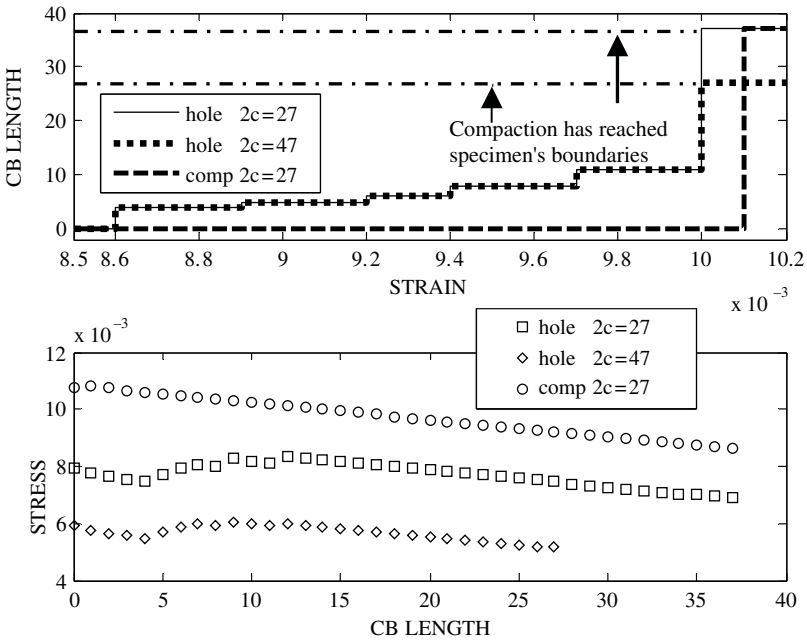

Fig. 5. (top) The cumulative length of a compaction band formed at the tips of holes of two different lengths, and at the tip of a preexisting CB, as a function of the remote external strain. When nucleating from the tip of a hole, compaction initiates at a lower strain (8.6×10^{-3}), and proceeds in a step-wise manner, till runaway starts at strain 10.0×10^{-3}. The curves for $2c=27$ and $2c=47$ (curves with two different lengths) coincide. When nucleating from the tip of a preexisting CB, compaction initiates at a higher strain of 10.1×10^{-3}, and proceeds through the whole sample at the same strain (runaway). (bottom) Macroscopic compressive stress, σ_L, as a function of cumulative length of the formed compaction band originating from a preexisting CB with a length of 27 units, and from the tips of holes with lengths of 27 and 47. In the specimen with the larger crack length ($2c=47$), compaction initiates at a macroscopic stress σ_L that is much smaller than in the specimen with the shorter crack ($2c=27$); during the runaway phase, the macroscopic stress, σ_L, subsides gradually, in a manner that is identical for both cracks and the CB, though for CBs runaway starts with nucleation, rather than later, as for the cracks (after about after 10 units of compaction).

5.2. Compaction bands in a specimen with an initial central crack

Fig. 4 presents development of CBs induced at the tip of an initial horizontal crack of length $2c$, in a specimen experiencing vertical compression. As strain is increased, CBs propagate incrementally (as in Vajdova et al., 2003; Vajdova and Wong, 2003) from the crack tip towards the lateral boundaries. This character of propagation is different than that observed above for a CB induced at the tip of an initial CB and in Katsman et al. (2005). There, new CBs were generated either by an elastic mismatch with the boundary, or by previously existing bands, and once compaction nucleated, CB propagation proceeded across the entire specimen width in a run-away mode.

In contrast, here (Fig. 4) it is observed that when compaction initiates at a crack tip, each macroscopic strain increment induces a finite increment of compaction. Compaction continues at the tip only after the remote macroscopic strain is increased again. The first and last increments of compaction (Fig. 5, top) result in compaction of more units than other increments.

5.3. Compaction bands in a specimen with initial notches

Figs. 6 and 7 present development of CBs induced by planar notches, each of length c, cut into the specimens' lateral boundaries (Fig. 3, bottom). Fig. 6 shows a simulation using a completely homogeneous specimen, whereas Fig. 7 shows results from a simulation with initial disorder D, following Eqs. (5) and (6).

Fig. 6 shows that at a certain strain, compaction initiates at the notch tip, followed by incremental CB propagation inward. The CB propagation scenario is identical to that induced by the initial central crack discussed above (Fig. 5). Fig. 7 shows CB development in a notched non-homogeneous specimen. Here disorder was introduced by using a small variability, $D=0.075$ (Eq. (6)). Simulations show a cluster of CBs (similar to diffuse CBs observed in Baud et al. (2004)) initiating at the notch tip in the sample's horizontal midsection, and propagating inwards. Outside this mid-section, no significant damage was observed. This scenario is reminiscent of the one demonstrated in Katsman et al. (2005) for a specimen with small disorder, elastic mismatch, and no initial defects. There a competition between two sources for compaction nucleation, namely elastic mismatch and disorder, resulted in dense compaction clusters. This manner of propagation coincides with that described in Vajdova et al. (2003) and Vajdova and Wong (2003). In general, the character of compaction propagation is very sensitive to the degree of sample heterogeneity. In simulations using larger disorder (not shown), $D>0.1$, CBs are arrested after propagating a very small distance away from the notches. Instead, diffuse compaction, distributed within the entire specimen volume, is nucleated, growing with increased macroscopic strain.

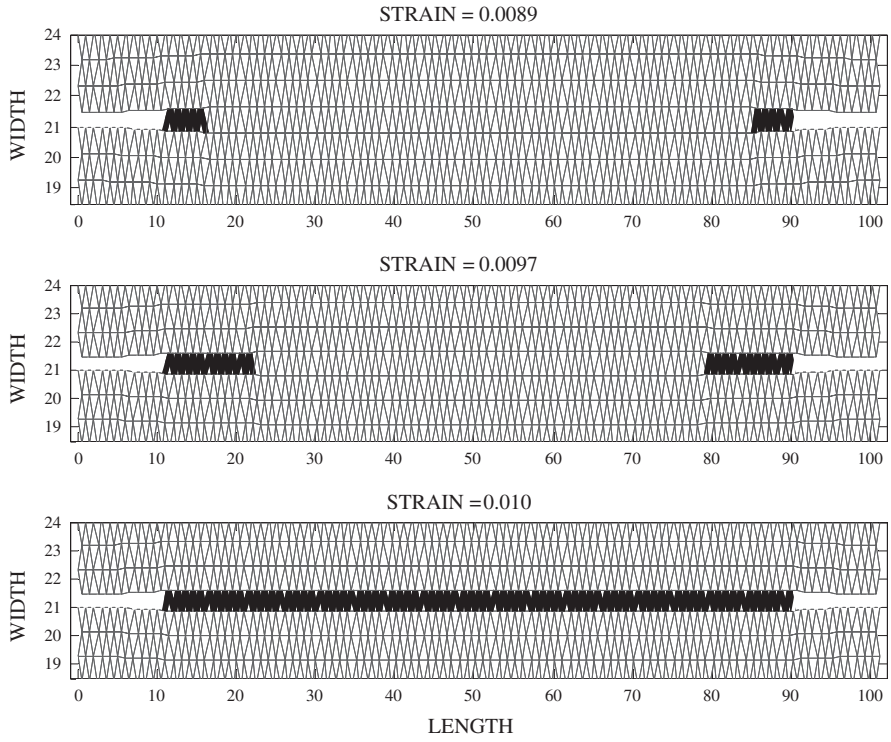

Fig. 6. Development of compaction bands induced by planar notches cut into the lateral boundaries of a completely homogeneous specimen ($D=0$). As strain increases, compaction bands propagate horizontally in an incremental fashion.

6. Discussion

The stress field within an elastic matter is a combination of the stress induced by defects (such as voids and CBs) and the imposed boundary stress. As a formed CB lengthens, the stress field evolves, in some cases causing variations in CB propagation rates (Fig. 5). In particular, it is possible to understand why CB propagation is incremental when initiated

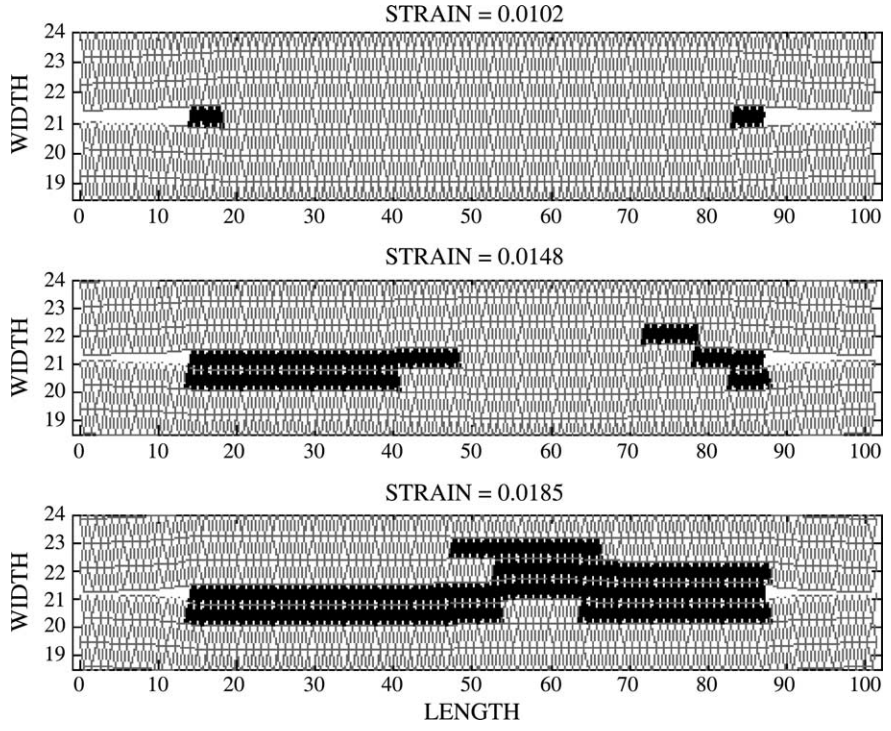

Fig. 7. Development of compaction bands induced by planar notches cut into the lateral boundaries of a non-homogeneous specimen ($D=0.075$). As strain increases, a cluster of compaction bands initiate at the notches tips, propagating incrementally inwards.

at a crack tip, versus runaway propagation when initiated at the tips of compressive defects, as explained below.

6.1. CB nucleation at the tip of defects

In order to compare CB nucleation at the tip of preexisting CBs and cracks, we need to understand the stress distribution around these two defects. Although the stress distribution around cracks is well understood and formulated analytically (e.g. Lawn and Wilshaw, 1975), only simulation results of the stress surrounding compaction bands are currently available.

Results of Katsman et al. (in press) show that stress around CBs is not similar to that around cracks, in either extension or compression (i.e. CBs are not similar to the anticracks described by Fletcher and Pollard (1981)). Instead, the vertical stress at the tip of a preexisting CB, σ_t (measured at the first unit adjacent to the CB), depends only very weakly on the CB length, $2c$. As shown by Katsman et al. (in press), σ_t is linearly related to the vertical volume reduction $2(H-h)$ (Fig. 1a and b), which occurred in the CB during compaction. In addition, it was shown that σ_t exceeds, by an almost constant value, the applied differential stress, σ_L (Fig. 8). As a result, an empirically derived form of the stress at the tip of a compaction band can be formulated as:

$$\sigma_t = (1 + \delta(\sigma_L, W, c))(\sigma_L + \alpha E e) \tag{7}$$

where E is the Young's modulus of the undamaged material, e is the plastic strain due to the compaction $e = (H-h)/H$, $2H$ is the pre-compacted height in the relaxed state (Fig. 1a and b), $2h$ is the post-compacted height in the relaxed state (Fig. 1a and b), related to the decrease in equilibrium length $\Delta l = l^{eq}_{old} - l^{eq}_{new}$ via

$$2(H-h) = \frac{\sqrt{3}}{2} \cdot l^{eq}_{old} - \sqrt{(l^{eq}_{old} - \Delta l)^2 - \frac{(l^{eq}_{old})^2}{4}} \tag{7a}$$

α is a proportionality coefficient (may also be derived from Eshelby (1957)), observed in the simulation of Katsman et al. (in press) to be approximately equal to 0.2, δ is a coefficient much smaller than 1, as demonstrated in Fig. 8, and W is the width of the sample.

The stress in the vicinity of a CB adjacent to a compressed void is quite different than in the absence of a void. The stress is a combination of (1) the large reversible compressive stress induced in the hole tip under compression—identical but opposite in sign to the stress induced at the hole tip under extension (Lawn and Wilshaw, 1975; Katsman et al., in press), (2) the generally smaller irreversible compression induced by the CB itself.

The normal stress of a crack of length $2c$ at a horizontal distance r away from a tip is well known:

$$\sigma(r) = M\sigma_L\sqrt{\frac{c}{2r}} \tag{8}$$

where M is a modification factor accounting for finite width of the elastic media (e.g. Lawn and Wilshaw, 1975). The parameter regime for which compression induced by a CB at its tip is smaller than that induced by a compressed crack at its tip may be found from Eqs. (7) and (8), using $r=1$ in Eq. (8), characterizing the distance between the middle of the last unit of the crack and the middle of the first undamaged unit adjacent to it. Thus CB tip stress is smaller than crack tip stress in cases when

$$\alpha E e < \sigma_L\left(M\sqrt{\frac{c}{2}} - 1\right) \tag{9}$$

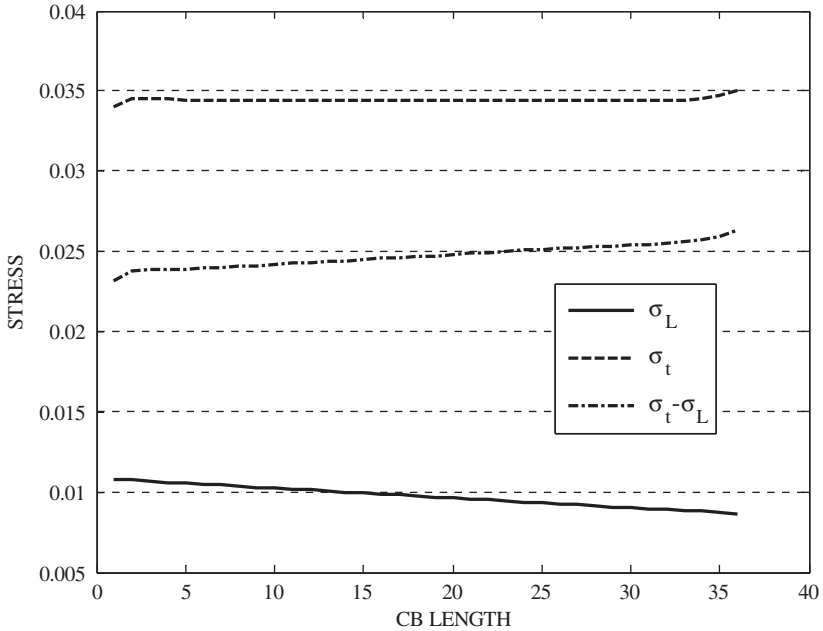

Fig. 8. The stress at a CB tip, σ_t, the applied differential stress, σ_L, and the difference between the two stresses $\sigma_t - \sigma_L$, as a function of the CB length. σ_t is observed to remain at an almost constant level above σ_L. The slope of $\sigma_t - \sigma_L$ is given by δ (Eq. (7)), which is seen to be much smaller than 1 and hence negligible.

(where δ in Eq. (7) was neglected). Under such conditions, which take place in our simulations, CBs initiate at the tips of cracks at a lower applied strain than those initiated at the tips of preexisting CBs. To demonstrate this we compare CBs nucleating at a tip of a preexisting crack of length $2c=27$, with CBs nucleating at the tip of a preexisting CB with the same initial length $2c=27$, using $\Delta l=0.1$ and $K_E=E_{new}/E_{old}=1.5$. It is found that for the same remote strain, the stress at the compaction band tip is much smaller than that at the crack tip. As a result, a CB at the tip of a crack (Fig. 4) initiates and starts propagating at much smaller remote strain (0.0086, Fig. 5, top) than the CB originating from a preexisting CB (strain 0.0101, Fig. 5, top).

From Eq. (8) it is also predicted that near cracks (but not near CBs) CB nucleation is dependent on crack length. This is because, to initiate compaction, the macroscopic strain and the resulting σ_L should be lifted to the value needed to cause compaction of the first unit adjacent to the hole only. At this point, the prescribed critical stress σ_{cr} at the first unit close to the crack tip is ($r=1$, Eq. (8)):

$$\sigma_{cr}=M\sigma_L\sqrt{\frac{c}{2}} \tag{10}$$

As a result, at constant σ_{cr}, the external load σ_L needed to nucleate compaction is inversely proportional to the square root of the crack length, i.e. compaction will initiate at lower remote macroscopic stresses for longer cracks:

$$\sigma_L=\frac{1}{M}\sigma_{cr}\sqrt{\frac{2}{c}} \tag{11}$$

To test the predictions of Eqs. (10) and (11), we compared CB initiation and propagation from the tips of two preexisting cracks with different lengths. As in all our simulations, the applied boundary conditions (in the Y direction) are constant strain-rate. At each step, the differential stress σ_L is calculated. Fig. 5 (bottom) shows that under the same remote macroscopic strain, specimens with larger initial crack length ($2c=47$), have smaller correspondent σ_L than specimens with shorter initial crack length ($2c=27$), as expected, because as cracks lengthen the matrix effectively softens. On the other hand, as Eq. (11) predicts, compaction initiates at lower σ_L for the longer crack, as shown in Fig. 5 (bottom). These two opposing effects ultimately led to compaction initiation at the same macroscopic strain (0.0086, Fig. 5, top) for both $2c=27$ and $2c=47$.

6.2. CB propagation after nucleation

In the case of a CB originating from a preexisting CB, stress is governed by Eq. (7). Because σ_t is independent of CB length, once compaction nucleates ($\sigma_t=\sigma_{cr}$), the band 'zips' through the entire sample, at the same strain. However, in an infinitely wide specimen held at constant strain boundary conditions, compaction must stop due to the σ_L decrease as compaction progresses (Fig. 5, bottom), leading to a decrease in σ_t (Eq. (7)).

When compaction is initiated at a crack tip, stress is first dominated by the presence of the void. The first compaction increment adjacent to the crack under compression is induced by the compressive stress σ_{cr} according to Eq. (10). After compaction of several units (Fig. 5), it is observed that compaction ceases to propagate. The arrest of compaction is mainly because stress decreases away from a crack tip as $1/\sqrt{r}$, causing σ_t to drop below σ_{cr}. However, when increasing the remote strain further, the stress induced by the crack tip is also increased, raising the stress in the next unit above σ_{cr}, thus leading to compaction of several more units, and so on. It is observed (fig.(5) upper) that this step-wise manner of propagation is independent of initial crack length. This can be understood from Eqs. (8) and (11); since the stress at a distance r away from the tip, at which σ_{cr} has been reached, is independent of crack length:

$$\sigma(r)=\sigma_{cr}\sqrt{\frac{1}{r}} \tag{12}$$

After the formed CB is long enough, and its tip is far enough from the crack tip, the crack-tip influence decays and the stress from the formed CB itself starts dominating, following Eq. (7). At a certain macroscopic strain, the prescribed stress for compaction threshold, σ_{cr}, is reached at the CB tip, i.e. $\sigma_t=\sigma_{cr}$, independent of the existing hole, and compaction propagates via the rest of the specimen, under the same strain, in a brittle run-away mode (the last 26 units in Fig. 5 (top), crack with $2c=27$), as seen by Katsman et al. (2005, in press).

During this runaway, although the macroscopic strain is held constant, the macroscopic differential stress σ_L subsides gradually (Fig. 5, bottom). In simulations using wider specimens, runaway is always seen according to this scenario (Fig. 5), crossing the entire specimen width, independently of specimen width and crack length. This runaway mode is similar to that occurring in the case of a CB propagating from a preexisting CB.

From our results and the above analysis, we presume that if small enough strain increments were used, the first increment of compaction adjacent to the hole will consist only of a single unit, proceeding in compaction of single units with slowly increasing strain, till runaway starts. Usage of such small strain increments leads to large cumulative numerical errors and time consumption, thus disabling such detailed calculations.

6.3. Comparison with experiments and field observations

Compaction propagation patterns simulated in this study under different conditions coincide with experimentally obtained patterns and field observations. In the experiments of Haimson et al., CBs propagate at a hole's tip in the direction perpendicular to the maximum compressive direction, as they did in our simulations. However, the Haimson et al. experiments had an added complexity: the de-bonded and compacted grains were removed by circulated fluids. As strain increased, the length of their emptied CB increased as well. According to our results, if material is not removed (the limit of low flow rate of the circulating fluid in Haimson et al.), the CB propagates incrementally, resulting in runaway propagation

only once CB length is large enough. If CB material is removed (high flow rate in the experiments), the stress at the empty CB tip will increase similarly to that of a lengthening crack, leading to accelerated propagation already from the compaction onset. Both trends coincide with the results of Haimson and Kovacich (2003). In practice, in high-porosity rock, the breakouts (emptied CBs) are seen (Haimson et al.) to propagate to very large distances without restrictions (contrary to breakouts in low-porosity rock, caused by a different mechanism), creating a highly non-homogeneous stress field due to a combination of emptied and compacted regions.

In contrast, in experiments of notched samples where the compacted matter was not removed, Vajdova et al. (2003) and Vajdova and Wong (2003) reported transverse CB propagation velocity only twice as fast as the axial displacement rate. This rate is also much slower than CB propagation induced by a stiff boundary (Olsson, 2001), where axial loading was termed quasistatic due to the CB runaway propagation in the transverse direction, followed by rapid compaction front propagation in the axial direction (front propagated at 8.3 times the axial displacement rate). The CB propagation rates from Vajdova et al. (2003), Vajdova and Wong (2003), and Olsson (2001) qualitatively coincide with our modeling, of a slower rate near a constant size notch versus a runaway mode induced by CB tips and other filled compressive defects.

Moreover, the morphology of the CBs observed in the field (Mollema and Antonellini, 1996; Sternlof et al., 2004), demonstrated incremental propagation of thick CBs, similar to the incremental propagation of the thick or diffuse CBs observed in notched samples, as demonstrated in Fig. 7. Specifically, under field conditions, the CBs nucleation may be induced by an initial crack or hole, whereas its large thickness is caused by the rock heterogeneity.

Finally, in Tembe et al. (in press), compaction in notched samples experimentally produced CBs at much lower differential stress than in unnotched samples, as predicted by our results when inequality (9) holds. Using numerical characteristics of porous rocks $E=20$ GPa, $e=0.1$, $\alpha=0.2$ (following our simulations results), it is found that the stress elevation above the applied stress, observed at a CB tip (αEe) is expected to be of the order of 400 MPa (Eq. (9)). When the applied differential stress is taken as $\sigma_L \sim 200$ MPa (Klein et al., 2001; Tembe et al., in press), inequality (9) holds for voids with non-dimensional length $c>18$. In dimensional units, this back of the envelope calculation predicts that CBs will grow for notches longer than 3.5 mm. This number is larger than the notch length of 2 mm observed by Tembe et al. (in press) to induce CBs. The differences may arise due to the following reasons. In Eq. (9), α leading to the large stress elevation of 400 MPa might be non-linear. Perhaps more importantly, the results obtained in two-dimensional calculations are likely to differ from the three-dimensional experimental conditions (Thorpe and Jasiuk, 1992). As a result, we predict that even small voids may induce a stress concentration at their tip which will initiate CBs. It is even possible that pores or microcracks in high porosity rocks play a role of stress concentrators that initiate CBs.

7. Conclusions

Both the modeling results presented here and our previous work (Katsman et al., 2005), study CB nucleation from defects in elastic matter. The main result presented here is explanation of the mechanism by which stress concentrations induced at the tips of pre-existing CBs and compressed voids may lead to CB formation. As a result, compaction induced by a pre-existing CB proceeds in a runaway manner. Compaction induced by a hole proceeds in a different, step-wise, manner. Compaction is expected to initiate (under most conditions) at lower remote strain when formed at the tip of a hole, rather than at the tip of a compaction defect, due to the generally larger stress concentrations existing near voids.

Compaction propagation is also sensitive to whether CBs remain filled, or are continuously emptied by fluids, since emptied CBs act as holes. Besides being a basic scientific question, and possibly controlling some aspects of basin compaction, CBs are an important issue in managing boreholes, where the formation of very long CBs may lead to considerable sand production and affect borehole stability in oil-producing fields.

Acknowledgements

This research is supported by a grant from BP. EA is an incumbent of the Anna and Maurice Boukstein Career Development Chair. We thank H. Scher, Z. Karcz, B. Haimson, and another anonymous reviewer for helpful suggestions.

Appendix A

SNMs exhibit a small odd–even asymmetry in the stress intensity, which is purely a consequence of the use of the hexagonal (triangular) network. The asymmetry occurs because the single non-horizontal springs belonging to either crack or CB tips interact with each other and the free surfaces differently in cases when the defects contain even or odd number of the springs (see Curtin and Scher (1990a,b) for the details). One way to eliminate this artifact is to consider the symmetric unit of a triangle of three springs rather than a single spring, as the basic unit. In practice this means that all quantities such as stress and strain are calculated independently for each spring, and then averaged over a triangular unit. In this case, the proper stress intensity scaling is preserved, and the stress concentrations are always maximal in the defect plane.

References

Baud, P., Klein, E., Wong, T.-f., 2004. Compaction localization in porous sandstones: spatial evolution of damage and acoustic emission activity. Journal of Structural Geology 26, 603–624.

Curtin, W.A., Scher, H., 1990a. Brittle fracture in disordered materials: a spring network model. Journal of Material Resources 5 (3), 535–553.

Curtin, W.A., Scher, H., 1990b. Mechanics modeling using a spring network. Journal of Material Resources 5 (3), 554–562.

Eshelby, J.D., 1957. The determination of the elastic field of an ellipsoidal inclusion, and related problems. Proceedings of the Royal Society of London (A), Mathematical and Physical Sciences 241 (1226), 376–396.

Fletcher, R.C., Pollard, D.D., 1981. Anticrack model for pressure solution surfaces. Geology 9, 419–424.

Haimson, B.C., 2001. Fracture-like borehole breakouts in high porosity sandstone: are they caused by compaction bands? Physics and Chemistry of the Earth (A) 26, 15–20.

Haimson, B.C., 2003. Borehole breakouts in Berea Sandstone reveal a new fracture mechanism. Pure and Applied Geophysics 160, 813–831.

Haimson, B.C., Kovacich, J., 2003. Borehole instability in high-porosity Berea sandstone and factors affecting dimensions and shape of fracture-like breakouts. Engineering Geology 69, 219–231.

Haimson, B.C., Lee, H., 2004. Borehole breakouts and compaction bands in two high-porosity sandstones. International Journal of Rock Mechanics & Mining Sciences 41, 287–301.

Issen, K.A., Rudnicki, J.W., 2000. Conditions for compaction bands in porous rock. Journal of Geophysical Research 105 (B9), 21529–21536.

Issen, K.A., Rudnicki, J.W., 2001. Theory of compaction bands in porous rock. Physics and Chemistry of the Earth (A) 26 (1-2), 95–100.

Katsman, R., Aharonov, E., Scher, H., 2005. Numerical simulation of compaction bands in high-porosity sedimentary rock. Mechanics of Materials 37 (1), 143–162.

Katsman, R., Aharonov, E., Scher, H., in press. A numerical study on localized volume reduction in elastic media: some insights on the mechanics of anticracks. Journal of Geophysical Research.

Klaetsch, A.R., Haimson, B.C., 2002. Porosity-dependent fracture-like breakouts in St. Peter sandstone. In: Hammah, R., Bawden, W., Curran, J., Telesnicki, M. (Eds.), Mining and Tunneling Innovation and Opportunity. University of Toronto Press, Toronto, pp. 1365–1371.

Klein, E., Baud, P., Reuschle, T., Wong, T.-f., 2001. Mechanical behavior and failure mode of Bentheim sandstone under triaxial compression. Physics and Chemistry of the Earth (A) 26 (1–2), 21–25.

Lawn, B.R., Wilshaw, T.R., 1975. Fracture of Brittle Solids. Cambridge University Press, Cambridge.

Mollema, P.N., Antonellini, M.A., 1996. Compaction bands: a structural analog for anti-mode I crack in Aeolian sandstone. Tectonophysics 267, 209–228.

Olsson, W.A., 2001. Quasistatic propagation of compaction fronts in porous rock. Mechanics of Materials 33, 659–668.

Rudnicki, J.W., Olsson, W.A., 1998. Reexamination of fault angles predicted by shear localization theory. International Journal of Rock Mechanics & Mining Sciences 35 (4/5), 512–513.

Schlangen, E., Garboczi, E.J., 1996. New method for simulating fracture using an elastically uniform random geometry lattice. International Journal of Engineering Science 34 (10), 1131–1144.

Schlangen, E., Garboczi, E.J., 1997. Fracture simulations of concrete using lattice models: computational aspects. Engineering Fracture Mechanics 57 (2/3), 319–332.

Sternlof, K., Pollard, D.D., 2002. Numerical modeling of compactive deformation bands as granular "anti-cracks". Eos Transactions AGU 83 (47), T11F-10.

Sternlof, K.R., Chapin, J.R., Pollard, D.D., Durlofsky, L.J., 2004. Permeability effects of deformation bands arrays in sandstone. AAPG Bulletin 88 (9), 1315–1329.

Tembe, S., Vajdova, V., Wong, T.-f., Zhu, W., in press. Initiation and propagation of strain localization in circumferentially notched samples of two porous sandstones. Journal of Geophysical Research.

Thorpe, M.F., Jasiuk, I., 1992. New results in the theory of elasticity for 2-dimensional composites. Proceedings of the Royal Society London, Series A 438, 531–544.

Vajdova, V., Wong, T.-f., 2003. Incremental propagation of discrete compaction bands: acoustic emission and microstructural observations on circumferentially notched samples of Bentheim. Geophysical Research Letters 30, 14 art. no. 1775.

Vajdova, V., Wong, T.-f., Farell, D.E., Issen, K.A., Challa, V., 2003. Experimental observation and numerical simulation of initiation and propagation of compaction bands in a sandstone. Proceedings ASCE Engineering Mechanics Conference, Seattle, July 16–18.

Wong, T.-f., David, C., Zhu, W., 1997. The transition from brittle faulting to cataclastic flow in porous sandstone: mechanical deformation. Journal of Geophysical Research 102, 3009–3025.

Wong, T.-f., Baud, P., Klein, E., 2001. Localized failure modes in compactant porous rock. Geophysical Research Letters 28 (13), 2521–2524.